

Efficient Condition-based Representations for Long-Term Visual Localization

Hugo Germain^{*1} Guillaume Bourmaud^{*2} Vincent Lepetit^{*1}

¹Laboratoire Bordelais de Recherche en Informatique, Université de Bordeaux, France

²Laboratoire IMS, Université de Bordeaux, France

Abstract

We propose an approach to localization from images that is designed to explicitly handle the strong variations in appearance happening when capturing conditions change throughout the day or across seasons. As revealed by recent long-term localization benchmarks, both traditional feature-based and retrieval-based approaches still struggle to handle such changes. Our novel retrieval-based method introduces condition-specific sub-networks allowing the computation of global image descriptors that are explicitly dependent of the capturing conditions. We compare our approach to previous localization methods on very recent challenging benchmarks, and observe that our method outperforms them by a large margin in case of day-night variation, where repeatable feature points cannot be identified or matched. Our code is made publicly available at <https://github.com/germain-hug/ECBR-Long-Term-Localization>.

1. Introduction

Outdoor environments are prone to large changes in visual appearance, both throughout the time of day and across longer periods of time. Such variations strongly impact the performance of image-based algorithms, for which visual localization is no exception. The goal of visual localization is to predict the 6 DoF camera pose for a visual query with respect to a reference frame. It is a crucial component of many robotic systems, including popular research areas like autonomous navigation [40] and augmented reality [41].

One interesting approach to visual localization is to cast it as an image-retrieval problem, sometimes also referred to as visual search. In this formulation, the unknown pose of the visual query is approximated using those of the top-ranked matches found in a geo-tagged database [2, 5, 13, 58]. Thus, the main goal of retrieval-based localization revolves around coming up with discriminative and robust image representations that are invariant

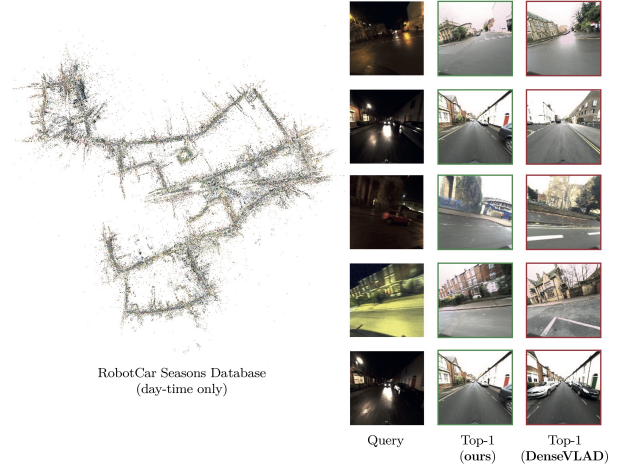


Figure 1: Overview of our approach: Given a pose-annotated image database captured in daytime only, our goal is to accurately relocalize query images captured in different and challenging conditions within this database. We introduce a simple and efficient architecture which explicitly considers the capturing conditions (day, night, etc.) of the query images to compute their descriptors, in order to localize them by retrieval. Our method (middle column) improves localization results at night time compared to traditionally used VLAD-based methods [2, 58] (right) by up to 42% on night images from RobotCar Seasons [48].

to large changes in viewpoint and scale, as well as long-term environment evolutions [2]. While inducing pose approximation, retrieval-based localization offers two key advantages. First, it is easily scalable to large environments. Compared to feature-based methods, we do not need to build and store a 3D model of the scene, but only the compact image descriptors which can further be compressed with quantization techniques [26]. Second, thanks to the global image descriptors robustness, retrieval-based localization currently outperforms traditional feature-based methods in night conditions at a coarse level of precision, as shown by recent benchmarks [48]. These two advantages

^{*}E-mail: {firstname.lastname}@u-bordeaux.fr

make this retrieval-based approach a suitable candidate for long-term visual localization.

In this paper, we consider the case where the reference images for a given location were captured under a very small number of conditions, maybe only one. This is a scenario very important in practice: For example, the reference images could be all captured during the same day, but should still be used to localize new images captured later on, at a different time of day or during a different season.

However, the overall performance of current retrieval methods [2, 58] for localization is still rather poor under varying conditions [48], and long-term visual localization is still far from being solved. Recent image-retrieval methods aim to learn an image representation independently from the capturing conditions, using a siamese or triplet architectures [2, 7, 21, 27, 43, 44, 57]. Unfortunately, current datasets only contain a limited amount of training samples per condition [8, 29, 48], and learning condition-invariant image descriptors remains challenging.

We therefore propose to make the computation of the image descriptors explicitly dependent of the capturing conditions. There are different possible ways to achieve this. Our solution is to split the network computing the descriptor for a given image in two parts. For simplicity, we consider a finite number of conditions, more exactly we consider the following conditions: rain, dawn, snow, dusk, sun, overcast in summer and winter, as well as night and rain at night-time. The first part of the network, performing image feature extraction, is different for each condition. This allows us to adapt to the variation of landmark appearances due to the conditions. The second part is the same for all the conditions. In this way, the final descriptor is learned by leveraging the complete training set. We show in our experiments that this is a very efficient and robust way to take into account the conditions when computing the image descriptor (see Figure 1).

We evaluate our approach on the very challenging RobotCar Seasons dataset [48], which provides accurately annotated reference images captured in daytime only, along with query images captured in multiple challenging conditions over the course of a full year [39].

2. Related Work

Visual localization methods usually fall into either of two categories: those leveraging a 3D model of the scene (*feature-based*), and those inferring the camera pose by retrieving the nearest image(s) in an annotated corpus (*retrieval-based*). We briefly review both approaches below in the context of long-term localization.

2.1. Feature-based localization

Traditional visual localization methods [33, 34, 36, 45, 50, 53] directly regress the full 6 DoF camera pose of

query images, with respect to a known reference. A typical pipeline of such feature-based methods includes acquiring a point-cloud model of the scene through *SfM*, and computing local feature descriptors like SIFT [37] or LIFT [60]. These descriptors are in turn used to establish 2D-to-3D correspondences with every point of the model, and the query’s camera pose can be directly inferred from those matches, using RANSAC [19, 49] combined with an Perspective-n-Point (PnP) solver [12, 22, 31].

Feature-based methods achieve very competitive results in consistent daytime conditions [47, 48, 50, 53, 59]. However, the pose estimation accuracy for such methods is heavily reliant on the local 2D-3D correspondences. Research in feature-based approaches mostly focuses on improving descriptor matching efficiency [15, 32, 33, 35, 38, 47], speed [18, 24] and robustness [34, 45, 46, 53, 54, 62]. Despite these efforts, a significant number of erroneous matches appear under strong appearance variations. As a result, dramatic drops in localization accuracy are observed in harder conditions such as night-time [48].

One workaround is to avoid using explicit feature matching altogether, and train a CNN to regress dense scene coordinates [10, 11, 28]. A confidence-ranking scheme such as DSAC [9] is then used to discard erroneous pose candidates sampled from the obtained depth map. However, such learning-based variants are hard to initialize [48, 51] and struggle with large environments [48]. Other direct learning-based variants include end-to-end pose regression from images [29, 59], although these approaches are overall less accurate [8, 10, 48].

Another way of making feature-based methods robust to condition perturbations is to use semantic reasoning. Semantic information can indeed be exploited to enhance either the feature matching stage [6, 30, 51, 52] or the pose estimation stage [56]. While being accurate at small scale, feature-based methods bottleneck is scalability. Both the construction of precise 3D models (and their maintenance), and local feature-matching is challenging and expensive in large-scale scenarios [50].

2.2. Retrieval-based localization

Retrieval-based or image-based localization methods trade-off accuracy for scalability, by modeling the scene as an image database, and visual localization as an image retrieval problem. Visual queries are matched with a pose-annotated images, using compact image-level representations. The query’s camera pose can then be simply inferred from the top-ranked images [13, 50, 61, 63], and the need for ground-truth 3D geometry is alleviated.

Robust global descriptors can be obtained by aggregation of local features in the image. VLAD [4] is a popular descriptor, computed by summing and concatenating many descriptors for affine-invariant regions. Den-

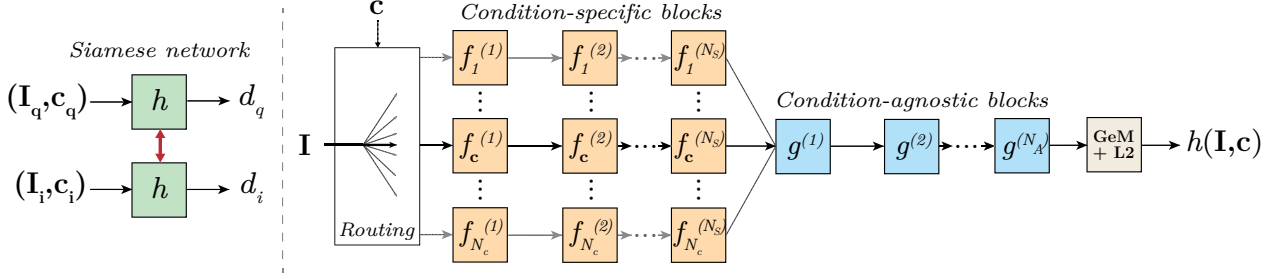


Figure 2: Detailed view of our siamese architecture. At a high level, our network is similar to a standard image-retrieval network, followed by a Generalized-Mean-Pooling (GeM) [43] activation and L2-normalization (see left). To exploit the image capturing condition, our network consists of N_S condition-specific blocks ($f_c^{(1)}, \dots, f_c^{(N_S)}$) for every condition, followed by N_A condition-agnostic blocks ($g^{(1)}, \dots, g^{(N_A)}$) (see right). When computing global image descriptors, inputs are routed to their appropriate condition-expert backbone. Note that the computational cost at inference time is independent of N_c , and the only additional cost is in terms of memory.

seVLAD [58] modified the VLAD architecture by densely sampling RootSIFT [3] descriptors in the image. Recent learning-based variants cast the task of image retrieval as a metric learning problem. NetVLAD [2] defines a differentiable VLAD layer as the final activation of a siamese network. While never explicitly applied to visual localization, activations such as max-pooling (MAC) [44, 57], sum-pooling (SPoC) [7], weighted sum-pooling (CroW) [27] or regional max-pooling (R-MAC) [21] coupled with siamese or triplet architectures, have shown to outperform VLAD-based methods in image-retrieval tasks [42]. The Generalized-Mean-Pooling (GeM) [43] layer proposes a hybrid activation, which combines the benefits of average and max-pooling, and achieves state-the-art results in outdoor visual search [42].

One bottleneck in retrieval-based localization is the spatially-sparse image sampling of the database. Three schemes can be implemented to compensate for the induced pose approximation: i) View synthesis [58] artificially generates intermediate samples, ii) relative pose regression [8, 55] acts as a separate refinement step, iii) multi-image methods [8, 61, 63] combine the top ranked images to improve pose accuracy.

Compared to 3D feature-based methods, retrieval-based methods offer two key advantages. First, the extension of such methods to city-scale scenarios is trivial [50]. Besides, in a very large database, unsupervised descriptor compression like PCA [25] or Product Quantization (PQ) [26] enables efficient approximate nearest-neighbour search with little loss in performance [21]. Secondly, evaluations in day-to-night [2, 58] or long-term [48, 56] visual localization reveal that retrieval-based methods outperform other feature-based methods like Active Search [47] at a coarse precision level. Image pre-processing [40] or translation [1] can be employed to bring all images to a visually similar and

condition-invariant representation. However, image translation methods are complex to train, require a full retraining for every condition and add to the overall computational cost of retrieval methods. Our method outperforms both retrieval and feature-based techniques without the need for such pre-processing.

3. Method

In this section, we give an overview of our pipeline.

3.1. Learning condition-based representations

As discussed in the introduction, we would like to train a method to compute a descriptor for a given image in a way that depends on the capturing conditions. We will exploit a training set made of images annotated with the 3D pose for the camera, and the capturing conditions:

$$\mathcal{D} = \{(I_i, c_i, M_i) \forall i \in (1, \dots, N)\}, \quad (1)$$

where $c_i \in \mathcal{C}$ is the capturing condition for I_i , and M_i is its camera pose. For simplicity, we assume a set \mathcal{C} of N_c finite and discrete capturing conditions, *i.e.* $\mathcal{C} = \{c_1, \dots, c_{N_c}\}$. In practice, we use the following set of conditions: rain, dawn, snow, dusk, sun, overcast in summer and winter, as well as night and rain at night-time. For supervised training purposes we define positive and negative labels $l(I_i, I_j) \in \{0, 1\}$, depending if the camera poses for I_i and I_j are close to each other or not. Details regarding those steps are provided in 4.2.

Many previous methods leverage a siamese or triplet network [2, 21, 27, 43, 44, 57]. Like the recent [43], we opt for a siamese architecture, mostly for its simplicity and we could also use a triplet network.

As shown in Figure 2, the key difference with previous approaches is that our architecture explicitly introduces

the capturing condition: When dealing with multiple conditions, traditional approaches define a single network to learn a joint representation across all capturing condition. While simple and compact, we argue that this approach struggles to handle strong appearance variations when given little training images per condition. Instead, we compute our image descriptor $h(I, c)$ for a given image I and its condition c with a network made of three components:

$$h(I, c; \Theta_1, \dots, \Theta_{N_c}, \Phi) = G\left(g\left(\prod_{i=1}^{N_c} f_i(I; \Theta_i)^{\delta(c-i)}; \Phi\right)\right). \quad (2)$$

where $\delta(\cdot)$ is the Dirac function. We have therefore N_c condition-specific sub-networks (f_1, f_2, \dots, f_{N_c}) of parameters $(\Theta_1, \Theta_2, \dots, \Theta_{N_c})$. Let us emphasize that during the forward pass, only the sub-network f_c corresponding to the condition c of the input image I is executed, *i.e.* in eq.(2) the Dirac function acts as a router. A second condition-agnostic sub-network g of parameters Φ takes the output of the network f_c as input. Function G denotes Generalized-Mean Pooling (GeM) [43] followed by L2 normalization. It is applied to the output of g to finally return a descriptor. This Generalized-Mean Pooling is discussed below.

G is parameter-free, and we train g and the f_c 's jointly by minimizing a contrastive loss function as in [14]:

$$\min_{\{\Theta_c\}_{c, \Phi}} \sum_{(I_i, c_i, I_j, c_j)} \mathcal{L}(I_i, c_i, I_j, c_j), \quad (3)$$

where

$$\mathcal{L}(I_i, I_j) = \begin{cases} l \|h(I_i, c_i) - h(I_j, c_j)\|^2 & \text{if } l(I_i, I_j) = 1 \\ \max\{0, m - \|h(I_i, c_i) - h(I_j, c_j)\|\}^2 & \text{otherwise,} \end{cases} \quad (4)$$

where $m > 0$ is a margin that can be set arbitrarily.

As a result of this optimization, the f_c networks become experts at mapping their specific conditions to a shared representation space, *with no additional computational cost at inference time compared to a standard pipeline.*

Generalized-Mean Pooling and Normalization. Final pooling layers of siamese networks are a key factor to generating robust and discriminative global image descriptors. The purpose of such layers is to efficiently aggregate local features into a fixed-length vector. Among existing techniques, the Generalized-Mean Pooling (GeM) [43] layer generalizes average [7] and global maximum pooling [44, 57], and has led to state-of-the-art results in learning-based image retrieval. We thus use it for our function G as the last component of h , together with a L2 normalization, instead of the more traditionally used VLAD-based representations [2, 58].

More exactly, let \mathcal{X} be a convolutional response of size $N \times M \times K$, and $\{\mathcal{X}_k, k \in (1, \dots, K)\}$ the set of $N \times M$

feature maps. We take:

$$G(\mathcal{X}) = \frac{\mathbf{d}}{\|\mathbf{d}\|}, \text{ where} \quad (5)$$

$$\mathbf{d} = \begin{pmatrix} d_1 \\ \vdots \\ d_K \end{pmatrix} \text{ with } d_k = \left(\frac{1}{|\mathcal{X}_k|} \sum_{x \in \mathcal{X}_k} x^{p_k} \right)^{\frac{1}{p_k}} \quad (6)$$

p_k acts as a factor between average ($p_k = 1$) and max-pooling ($p_k \rightarrow \infty$). The resulting global descriptors have proved to be highly discriminative and to deliver state-of-the-art results in challenging datasets [42].

3.2. Localization by retrieval

Finally, we perform localization by approximating the query pose with the one of the top-ranked image. We pre-compute normalized global descriptors for every image in the database using the aforementioned method, and find the nearest image by cosine similarity with the query's descriptor. To remove descriptor noise due to over-represented features, we learn and apply descriptor whitening discriminatively using our training data [43]. More specifically, we subtract the mean GeM vector μ and rescale the descriptors using the covariance estimated from positive samples.

4. Experimental Setup

4.1. Dataset

We train and evaluate our approach on the 'RobotCar Seasons' dataset made by Sattler *et al.* [48], which is a revision of the Oxford RobotCar dataset [39]. The original Oxford RobotCar dataset consists of outdoor urban images captured from a car and over the course of a full year, across overlapping trajectories. It features both short-term (*e.g.* day-to-night, weather) and long-term (*e.g.* seasonal) environment evolutions, and therefore different conditions. Images were captured as triplets along three fixed viewpoints (left, rear, and right).

The RobotCar Seasons refines a subset of the original dataset by recomputing pose annotations more accurately (using LIDAR scans, INS, SfM and manual annotation), and by labelling images with discrete capturing conditions. The release of this new dataset came along with a new benchmark, aiming specifically at evaluating visual localization algorithms robustness to strong appearance changes.

More exactly, the RobotCar Seasons dataset is split in three separate groups. The first one, which we refer to as *mixed-conditions*, consists of 5,718 pose-annotated images equally distributed across 9 different capturing conditions. The second one, called *overcast-reference*, is made of 20,862 pose-annotated images captured in a single traversal. The latter group of images is provided along with a corresponding 3D point cloud of the scene. Lastly, the *query*



Figure 3: Example query with its associated positive samples from *mixed-conditions*, obtained through condition-balanced hard mining with relaxed inliers.

group, which we evaluate ourselves on, consists of 6,216 queries captured under multiples conditions, which overlap with the *overcast-reference* traversal. This makes our approach challenging because we cannot leverage cross-condition information for the reference traversal, and thus need to generalize appearance variations on spatially separate information. In our evaluation, we always make predictions using single images at a time and do not leverage associated triplets to infer the query camera pose.

4.2. Training Set

In order to train our image retrieval pipeline, we need to define a set of relevant positive (visually overlapping) and negative (with no co-visibility) samples for every training query. We build our dataset using hard positive and negative mining.

Positive samples: To generate positive samples, we randomly sample images from *mixed-conditions* and *overcast-reference*, which share sufficient co-visibility with the query—this method was referred to as ‘relaxed inliers’ in [43]. Randomly sampling within the positive set ensures high variance in viewpoints, while the co-visibility constraint preserves reasonable scale changes. For *overcast-reference* images, we have access to a 3D representation of the scene. Let $p(I_i)$ be the set of visible 3D points in I_i , the positive samples for image I_q with relaxed inliers mining are given by:

$$\mathcal{P}_q = \left\{ (I_i, c_i) : \frac{|p(I_i) \cap p(I_q)|}{|p(I_q)|} > t_i, i \in [1, N], i \neq q \right\} \quad (7)$$

We use a value of $t_i = 0.6$.

Condition-balanced positive samples: For images in *mixed-conditions*, we do not have access to a 3D representation of the scene. Thus, we define the set of positives by randomly sampling within poses that fall under translation and orientation distance thresholds. Let (R_i, T_i) be the absolute camera pose of I_i , the positive samples for image I_q captured under condition j with relaxed inliers mining are given by:

$$\mathcal{P}_q^j = \left\{ (I_i, c_i) : \begin{cases} \text{dist}(R_i, R_j) < t_R \\ \text{dist}(T_i, T_j) < t_T \\ c_i = j \end{cases}, i \in [1, N], i \neq q \right\} \quad (8)$$

c_i	Conditions	Number of images	Total per sub-branch
$c_i = 0$	dawn	690	690
$c_i = 1$	snow	717	717
$c_i = 2$	sun	627	627
$c_i = 3$	night	591	1,263
	night-rain	672	
$c_i = 4$	overcast-summer	660	3,266
	overcast-winter	606	
	overcast-reference	20,862*	
$c_i = 5$	dusk	561	1,155
	rain	594	

Table 1: Capturing condition binning of the training set. To avoid diluting images across too many sub-networks f_c , we merge some conditions based on visual similarity (* Due to the relatively large number of images in *overcast-reference*, 2,000 images from the 20,862 are resampled at every epoch).

We use a value of $t_R = 10^\circ$ and $t_T = 8m$.

To ensure a balanced distribution across capturing conditions within *mixed-conditions*, we sample the same number of positive samples for every condition $j \in \{c_1, \dots, c_{N_c}\}$. Doing so helps regulating over-represented conditions within the training set. See Figure 3 for an example of positive samples obtained with this technique. As shown in Table 1, there are far more images in *overcast-reference* than in each condition of *mixed-conditions*, and we only use a subset of 2,000 samples from *overcast-reference*, which we resample at every epoch.

Negative samples and pose approximation: We define the set of negative samples as the images which do not present any visual overlap. We pre-compute the negative samples for every query and perform hard-negative mining at every epoch to identify the most challenging images.

Our final sample can be written as the t-uple $(I_q, I_{p_1}, \dots, I_{p_P}, I_{n_1}, \dots, I_{n_N})$. We use $P = 8, N = 8$. We found that applying both mining techniques was crucial to speed up the convergence and make retrieval robust to viewpoint changes. However, due to the sampling step in positive mining, we also induce a greater pose approximation when estimating the query pose from top-1 images.

Condition binning: RobotCar Seasons offers a total of 10 capturing conditions, with the *night* and *night-rain* being the most challenging ones [48]. While defining a condition-specific backbone for every condition could potentially lead to a more accurate representation pre-processing, this also results in having fewer training samples per sub-branch. Therefore, to increase the number of training samples per backbone, we choose to merge some of the capturing con-

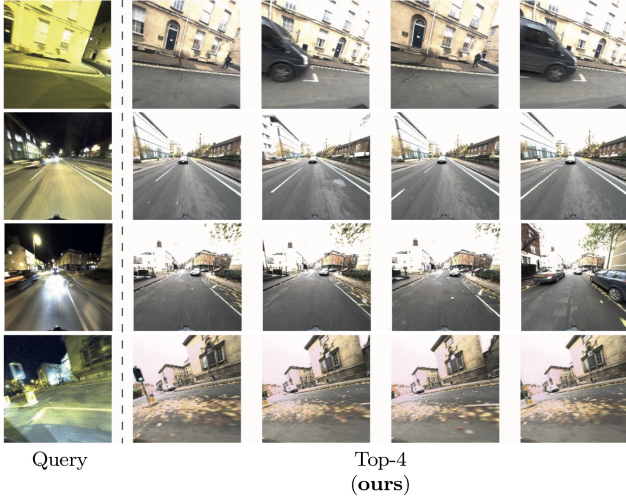


Figure 4: Top-4 retrieval results for night-time queries. Our method successfully finds query images despite strong illumination and overall appearance changes.

ditions based on their visual similarity. We set $N_C = 6$ and combine branches following the repartition presented in Table 1. RobotCar Seasons provides us with very accurate poses, but little training samples per conditions (about 600 images per condition). As a result even when merging conditions, generalizing to unseen places captured under challenging conditions remains particularly hard.

4.3. Image-retrieval Pipeline

We train and evaluate our approach on several network architecture variants, followed by some descriptor post-processing steps.

Architectures: Considering a ResNet-50 [23] with weights initialized from ImageNet [17], coupled with a GeM activation (set with $p_k = 3$) followed by $L2$ -normalization, let N_S be the number of condition-specific blocks. Each condition-specific branch f_{c_i} for $c_i \in \{c_1, \dots, c_{N_c}\}$ is therefore made of N_S blocks. We first define a baseline such that $N_S = 0$. This results in a traditional siamese network identical to [43], which although popular in image retrieval has not been evaluated so far for the task of visual localization. Then, we train three additional pseudo-siamese networks with $N_S = 2, 3, 4$. When $N_S = 4$, we end up with N_c separated ResNet-50 being trained jointly. Training is run for 20 epochs, on images rescaled to a resolution of 512×512 . Details about the number of parameters used for each variant can be found in supplementary material.

Lastly, one could argue that when $N_S \neq 0$, implicit information on the capturing condition is being propagated until the merging point of the subnetworks. For a fair comparison and to mimic this propagation, we subsequently

N_S	Backbone	Multi-Scale	Day-All			Night-All		
			Threshold Accuracy (%)			Threshold Accuracy (%)		
			0.25m 2°	0.5m 5°	5m 10°	0.25m 2°	0.5m 5°	5m 10°
0	ResNet-50		4.99	20.51	88.01	0.93	3.03	37.76
0	ResNet-50	✓	5.20	20.72	89.26	1.63	5.59	52.45
2	ResNet-50		6.58	23.42	88.22	1.40	3.73	46.62
2	ResNet-50	✓	6.03	23.08	89.40	1.16	5.36	53.61
3	ResNet-50		5.27	20.65	85.65	0.93	3.26	48.02
3	ResNet-50	✓	4.99	19.47	88.08	1.16	5.36	54.08
4	ResNet-50		4.85	19.26	83.58	0.93	3.96	50.82
4	ResNet-50	✓	4.85	18.99	86.56	1.40	6.06	58.74
0	ResNet-101	✓	4.44	18.02	83.09	1.63	4.20	41.72

Table 2: Ablation study of our approach on day-time and night-time images. We compare the effects of making more resnet blocks condition-specific, as well as the impact of adding pose multi-scale inference and using a larger backbone.

trained a ResNet-50 with concatenated channels at the entry of each block, containing a discrete label representing the capturing conditions. However, despite our efforts and with weights initializations both from ImageNet [17] and from Xavier [20], we were not able to make this model converge properly and retrieve images correctly.

Post-processing: To improve retrieval at inference time, we follow commonly used post-processing steps in image retrieval. First, we learn and apply whitening [25] in a discriminative fashion, as in [43]. Doing so helps dealing removing noise in descriptors coming from over-represented occurrences. In addition, we follow the multi-scale descriptor aggregation proposed by [43], to combine descriptors coming from rescaled inputs using the GeM layer. We feed inputs of size 512×512 , 724×724 and 1024×1024 pixels.

4.4. Evaluation

We evaluate our approach using the same localization metric as [48]. Three positional and rotational precision thresholds are defined (0.25m and 2°; 0.5m and 5°; 5m and 10°) and we report the percentage of query images correctly localized within those thresholds. Such binning of localization accuracy is a rather harsh metric for our retrieval-based methods, as they are dependent on the dataset sampling and may not systematically find the nearest image but its neighbors slightly further away. Therefore, we also provide cumulative distributions over the translation and orientation errors under several capturing conditions (see Figure 5). We compare ourselves against 2D retrieval-based methods like NetVLAD [2], DenseVLAD [58] and FAB-MAP [16]. In addition, we present results from structure-based methods, which require an additional pre-acquired 3D model of the scene. Such methods include Active Search [47], CSL [53] and a recent variant of Active Search combined with Semantic Matching Consistency [56].

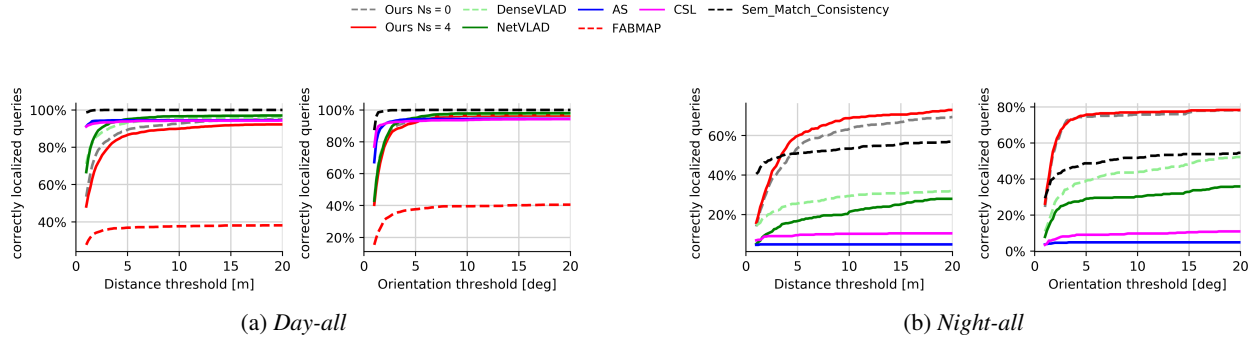


Figure 5: Cumulative distributions over the translation and rotation errors for day-time and night-time categories. Our method is slightly under state-of-the-art methods across all day-time conditions, but shows significant improvements at night-time.

		Day-All			Night-All		
Method	Threshold Accuracy (%)	0.25m	0.5m	5m	0.25m	0.5m	5m
		2°	5°	10°	2°	5°	10°
Feature-based	CSL [53]	54.54	85.93	93.35	0.70	3.26	9.32
	Active Search [47]	44.14	80.60	94.32	0.93	3.03	4.90
	AS + Sem. Match [56]	58.90	93.00	100.00	8.86	29.84	49.88
Retrieval-based	FAB-MAP [16]	3.12	13.37	36.73	0.0	0.0	0.0
	NetVLAD [2]	8.32	31.32	94.94	0.23	1.40	15.85
	DenseVLAD [58]	9.77	36.11	93.00	1.63	5.13	24.71
Ours ($N_S = 4$)		4.85	18.99	86.56	1.40	6.06	58.74

Table 3: Localization results on of the RobotCar Seasons dataset [48]. In this table, we present results across all 7 day-time categories (*Day-all*) and night-time categories (*Night-all*). We report the percentage of correctly localized images within three precision thresholds for our approach, as well as state-of-the-art methods. We distinguish feature-based methods like Active Search (AS), CSL, and AS combined with semantic reasoning—which require a 3D model of the scene—from retrieval-based FAB-MAP, NetVLAD, and DenseVLAD—which do not. Feature-based methods achieve state-of-the-art results on day-time images, while our approach outperform all existing methods on nigh-time images at a precision superior to 3m and 2.5°.

5. Results

In this section, we present the results of our localization experiments run on the architectures mentioned earlier. We start with an ablation study, followed by a comparison with both retrieval-based and feature-based state-of-the-art methods.



Figure 6: Example of failure cases on RobotCar Seasons. Some night-time query images are particularly dark with strong motion blur, making them extremely hard to retrieve.

5.1. Ablation Study

In Table 2, we compare the impact of several factors in our architecture. First, we evaluate the effect of increasing N_S , *i.e.* making more blocks condition-specific. We find that on very challenging conditions such as night-time images, the network benefits from more computational power dedicated to that condition. In fact, the optimal architecture for night-time is obtained when all blocks are condition-specific, meaning each condition leverages a full ResNet-50. On the other hand, we find that doing so slightly decreases overall performance in day-time. More specifically, conditions which only have a few samples to train on (*dawn*, *snow*, *sun*) do not benefit from deeper dedicated layers and tend to overfit, while sub-branches which have more training data (*dusk*, *overcast-summer*) tend to improve retrieval on such images. Overall, we find that conditions that are particularly hard require a larger amount of condition-specific blocks, while easier conditions will benefit more from having more samples to train and more condition-agnostic blocks. As a result, we have a trade-off in performance between N_S and the size and distribution of our training set across conditions.

We also consistently observe that using multi-scale inputs shows mild to strong performance increases. Lastly, we find that using a single larger network such as ResNet-101 damages the results, most likely due to overfitting with

		Day-All																				
		Rain			Dawn			Snow			Dusk			Sun			Overcast-summer			Overcast-winter		
Method		Threshold Accuracy			Threshold Accuracy			Threshold Accuracy			Threshold Accuracy			Threshold Accuracy			Threshold Accuracy			Threshold Accuracy		
		0.25m 2°	0.5m 5°	5m 10°	0.25m 2°	0.5m 5°	5m 10°	0.25m 2°	0.5m 5°	5m 10°	0.25m 2°	0.5m 5°	5m 10°	0.25m 2°	0.5m 5°	5m 10°	0.25m 2°	0.5m 5°	5m 10°	0.25m 2°	0.5m 5°	5m 10°
Feature-based	CSL [53]	73.17	94.63	100.00	54.19	89.43	96.92	61.40	94.88	97.21	75.13	95.43	100.00	33.93	52.68	70.98	37.44	82.94	91.47	48.17	96.34	100.00
	Active Search [47]	66.34	91.71	99.51	42.73	87.67	98.68	42.33	84.65	98.60	57.87	86.80	100.00	33.04	53.13	71.88	28.91	73.93	94.31	39.02	90.24	100.00
	AS + Sem. Match [56]	78.05	94.63	100.00	56.39	94.71	100.00	60.46	97.67	100.00	72.59	94.92	100.00	52.23	80.80	100.00	44.55	93.84	100.00	47.56	95.73	100.00
Retrieval-based	FAB-MAP [16]	12.20	40.49	92.20	2.20	5.29	10.57	3.26	8.84	28.37	2.54	18.27	57.36	0.00	0.00	0.89	0.95	9.48	30.81	0.61	14.02	46.34
	NetVLAD [2]	12.20	46.83	100.00	10.13	28.19	87.67	8.84	32.56	95.35	4.57	25.38	97.46	8.48	22.77	88.84	9.95	35.07	97.63	2.44	28.66	100.00
	DenseVLAD [58]	13.66	50.73	100.00	15.42	45.81	97.36	10.23	38.14	93.49	7.61	35.53	98.48	8.04	22.32	78.13	9.00	30.33	88.15	2.44	28.66	97.56
	Ours ($N_S = 4$)	7.32	26.34	98.54	4.85	19.38	76.65	4.65	20.47	89.30	3.55	20.30	94.42	4.91	13.84	78.57	7.11	18.01	82.94	0.61	14.02	87.80

Table 4: Day-time localization results (values from [48] accounting for the *mixed-conditions* additional training images). We report localization performance for our approach, as well as state-of-the-art feature-based (Active Search, CSL, Active Search with semantic reasoning) and retrieval-based (FAB-MAP, NetVLAD, DenseVLAD) methods.

		Night-All					
		Night			Night-Rain		
Method		Threshold Accuracy (%)			Threshold Accuracy (%)		
		0.25m 2°	0.5m 5°	5m 10°	0.25m 2°	0.5m 5°	5m 10°
Feature-based	CSL [53]	0.44	1.33	6.19	0.99	5.42	12.81
	Active Search [47]	0.88	2.21	3.54	0.99	3.94	6.40
	AS + Sem. Match [56]	10.18	26.54	50.80	7.39	33.50	48.77
Retrieval-based	FAB-MAP [16]	0.0	0.0	0.0	0.0	0.0	0.0
	NetVLAD [2]	0.00	0.88	18.14	0.49	1.97	13.30
	DenseVLAD [58]	0.88	4.42	24.34	2.46	5.91	25.12
	Ours ($N_S = 4$)	0.88	4.42	56.19	1.97	7.88	61.58

Table 5: Night-time localization results (values from [48] accounting for the *mixed-conditions* additional training images) for our approach and state-of-the-art feature-based and retrieval-based methods.

the little training data we are provided with. Thus, using a larger architecture naively does not correlate with performance improvement, and our method deals with hard conditions much more effectively.

5.2. Comparison with state-of-the-art

Tables 3, 4, 5 show localization results on the Robot-Car Seasons [48] dataset across all capturing conditions. Our baseline with $N_S = 0$ corresponds to the architecture with no condition-specific blocks. It outperforms both retrieval-based approaches at night-time, and feature-based for coarse precision thresholds. This first improvement can be attributed to the discriminative power of the GeM [43] layer combined with an efficient and condition-balanced positive and negative mining (see Section 4.2). However, this network achieves slightly less accurate localization in day-time conditions, compared to other retrieval methods like NetVLAD [2] or DenseVLAD [58]. This can be

explained by the way positive samples were constructed, which does not enforce returning the spatially closest image, but merely one that presents sufficient visual overlap.

Compared to the baseline, when $N_S = 4$ our method further increases night-time localization for coarse (5m, 10°) and medium (0.5m, 5°) thresholds by 6.29% and 0.47% respectively. Compared to DenseVLAD [58], this increases the results by 237% for coarse precision, and by 1200% compared to AS [47]. See Figure 4 for qualitative results.

Day-time localization is still widely dominated by feature-based methods like CSL [53] or Active Search [47], which efficiently leverage accurate large-scale 3D models of the scene. In day-time conditions, feature-based methods are especially relevant under high-precision regimes, where retrieval-based methods are limited by the dataset spatial sampling resolution. However, as observed under challenging conditions like *night*, *night-rain* or even *sun* where image are blown out, feature-based methods are prone to failure. Indeed, local descriptors are very sensitive to strong changes in appearance, where global image descriptors such as the ones produced by our approach can efficiently withstand such perturbations. Semantic reasoning as done in [56] helps rejecting outliers in feature-based methods, but this requires a 3D model of the scene that needs to be captured and maintained as discussed in the introduction.

6. Conclusion and Future Work

We have presented a novel image-retrieval architecture for visual localization which efficiently and explicitly handles strong appearance variations. We showed that our method widely outperforms both state-of-the-art feature-based and retrieval-based methods for night-time localization. Moreover, our method introduces no additional computational cost at inference time compared to a standard siamese pipeline.

However, retrieval-based methods alone still struggle to

achieve competitive localization results at day-time, but provide a more robust pose initialization. Improving the accuracy of the predicted pose of retrieval-based methods is therefore the next logical step, and will require being able to align the query image with the retrieved reference image under different conditions.

Acknowledgement

This project has received funding from the Bosch Research Foundation (Bosch Forschungsstiftung). The authors would also like to thank Torsten Sattler for providing support and evaluation tools with the RobotCar Seasons dataset [48].

References

- [1] A. Anosheh, T. Sattler, R. Timofte, M. Pollefeys, and L. V. Gool. Night-to-day image translation for retrieval-based localization. *CoRR*, abs/1809.09767, 2018. 3
- [2] R. Arandjelovic, P. Gronát, A. Torii, T. Pajdla, and J. Sivic. Netvlad: Cnn architecture for weakly supervised place recognition. *IEEE Conference on Computer Vision and Pattern Recognition (CVPR)*, pages 5297–5307, 2016. 1, 2, 3, 4, 6, 7, 8
- [3] R. Arandjelovic and A. Zisserman. Three things everyone should know to improve object retrieval. *IEEE Conference on Computer Vision and Pattern Recognition*, pages 2911–2918, 2012. 3
- [4] R. Arandjelovic and A. Zisserman. All about vlad. *IEEE Conference on Computer Vision and Pattern Recognition*, pages 1578–1585, 2013. 2
- [5] R. Arandjelovic and A. Zisserman. Dislocation: Scalable descriptor distinctiveness for location recognition. In *ACCV*, 2014. 1
- [6] R. Arandjelovic and A. Zisserman. Visual vocabulary with a semantic twist. In *ACCV*, 2014. 2
- [7] A. Babenko and V. S. Lempitsky. Aggregating local deep features for image retrieval. *2015 IEEE International Conference on Computer Vision (ICCV)*, pages 1269–1277, 2015. 2, 3, 4
- [8] V. Balntas, S. Li, and V. Prisacariu. Relocnet: Continuous metric learning relocalisation using neural nets. In *The European Conference on Computer Vision (ECCV)*, 09 2018. 2, 3
- [9] E. Brachmann, A. Krull, S. Nowozin, J. Shotton, F. Michel, S. Gumhold, and C. Rother. Dsac — differentiable ransac for camera localization. *2017 IEEE Conference on Computer Vision and Pattern Recognition (CVPR)*, pages 2492–2500, 2017. 2
- [10] E. Brachmann and C. Rother. Learning less is more - 6d camera localization via 3d surface regression. *CoRR*, abs/1711.10228, 2017. 2
- [11] M. Bui, S. Albarqouni, S. Ilic, and N. Navab. Scene coordinate and correspondence learning for image-based localization. In *BMVC*, 2018. 2
- [12] M. Bujnak, Z. Kukelova, and T. Pajdla. New efficient solution to the absolute pose problem for camera with unknown focal length and radial distortion. In *ACCV*, 2010. 2
- [13] D. M. Chen, G. Baatz, K. Köser, S. S. Tsai, R. Vedantham, T. Pylvänäinen, K. Roimela, X. Chen, J. Bach, M. Pollefeys, B. Girod, and R. Grzeszczuk. City-scale landmark identification on mobile devices. *CVPR 2011*, pages 737–744, 2011. 1, 2
- [14] S. Chopra, R. Hadsell, and Y. LeCun. Learning a similarity metric discriminatively, with application to face verification. In *IEEE Conference on Computer Vision and Pattern Recognition*, volume 1, 2005. 4
- [15] S. Choudhary and P. J. Narayanan. Visibility probability structure from sfm datasets and applications. In *Proceedings of the 12th European Conference on Computer Vision - Volume Part V, ECCV’12*, pages 130–143, Berlin, Heidelberg, 2012. Springer-Verlag. 2
- [16] M. J. Cummins and P. Newman. Fab-map: Probabilistic localization and mapping in the space of appearance. *I. J. Robotics Res.*, 27:647–665, 2008. 6, 7, 8
- [17] J. Deng, W. Dong, R. Socher, L.-J. Li, K. Li, and L. Fei-Fei. ImageNet: A Large-Scale Hierarchical Image Database. In *CVPR09*, 2009. 6
- [18] M. Donoser and D. Schmalstieg. Discriminative feature-to-point matching in image-based localization. *2014 IEEE Conference on Computer Vision and Pattern Recognition*, pages 516–523, 2014. 2
- [19] M. A. Fischler and R. C. Bolles. Random sample consensus: A paradigm for model fitting with applications to image analysis and automated cartography. *Commun. ACM*, 24:381–395, 1981. 2
- [20] X. Glorot and Y. Bengio. Understanding the difficulty of training deep feedforward neural networks. In *In Proceedings of the International Conference on Artificial Intelligence and Statistics (AISTATS’10). Society for Artificial Intelligence and Statistics*, 2010. 6
- [21] A. Gordo, J. Almazán, J. Revaud, and D. Larlus. End-to-end learning of deep visual representations for image retrieval. *International Journal of Computer Vision*, 124:237–254, 2017. 2, 3
- [22] R. M. Haralick, C.-N. Lee, K. Ottenberg, and M. Nölle. Review and analysis of solutions of the three point perspective pose estimation problem. *International Journal of Computer Vision*, 13:331–356, 1994. 2
- [23] K. He, X. Zhang, S. Ren, and J. Sun. Deep residual learning for image recognition. *2016 IEEE Conference on Computer Vision and Pattern Recognition (CVPR)*, pages 770–778, 2016. 6
- [24] I. Heisterklaus, N. Qian, and A. Miller. Image-based pose estimation using a compact 3d model. *2014 IEEE Fourth International Conference on Consumer Electronics Berlin (ICCE-Berlin)*, pages 327–330, 2014. 2
- [25] H. Jégou and O. Chum. Negative evidences and co-occurrences in image retrieval : the benefit of pca and whitening. 2012. 3, 6
- [26] H. Jégou, M. Douze, and C. Schmid. Product quantization for nearest neighbor search. *IEEE Transactions on Pattern Analysis and Machine Intelligence*, 33:117–128, 2011. 1, 3
- [27] Y. Kalantidis, C. Mellina, and S. Osindero. Cross-dimensional weighting for aggregated deep convolutional features. In *ECCV Workshops*, 2016. 2, 3
- [28] A. Kendall and R. Cipolla. Geometric loss functions for cam-

- era pose regression with deep learning. *2017 IEEE Conference on Computer Vision and Pattern Recognition (CVPR)*, pages 6555–6564, 2017. 2
- [29] A. Kendall, M. K. Grimes, and R. Cipolla. Posenet: A convolutional network for real-time 6-dof camera relocation. *2015 IEEE International Conference on Computer Vision (ICCV)*, pages 2938–2946, 2015. 2
- [30] N. Kobyshev, H. Riemenschneider, and L. V. Gool. Matching features correctly through semantic understanding. *2014 2nd International Conference on 3D Vision*, 1:472–479, 2014. 2
- [31] Z. Kukelova, M. Bujnak, and T. Pajdla. Real-time solution to the absolute pose problem with unknown radial distortion and focal length. *2013 IEEE International Conference on Computer Vision*, pages 2816–2823, 2013. 2
- [32] V. Larsson, J. Fredriksson, C. Toft, and F. Kahl. Outlier rejection for absolute pose estimation with known orientation. In *BMVC*, 2016. 2
- [33] Y. Li, N. Snavely, and D. P. Huttenlocher. Location recognition using prioritized feature matching. In *Proceedings of the 11th European Conference on Computer Vision: Part II, ECCV’10*, pages 791–804, Berlin, Heidelberg, 2010. Springer-Verlag. 2
- [34] Y. Li, N. Snavely, D. P. Huttenlocher, and P. Fua. Worldwide pose estimation using 3d point clouds. In *Large-Scale Visual Geo-Localization*, 2012. 2
- [35] H. Lim, S. N. Sinha, M. F. Cohen, and M. Uyttendaele. Real-time image-based 6-dof localization in large-scale environments. *2012 IEEE Conference on Computer Vision and Pattern Recognition*, pages 1043–1050, 2012. 2
- [36] L. Liu, H. Li, and Y. Dai. Efficient global 2d-3d matching for camera localization in a large-scale 3d map. *2017 IEEE International Conference on Computer Vision (ICCV)*, pages 2391–2400, 2017. 2
- [37] D. G. Lowe. Distinctive image features from scale-invariant keypoints. *Int. J. Comput. Vision*, 60(2):91–110, Nov. 2004. 2
- [38] S. Lynen, T. Sattler, M. Bosse, J. A. Hesch, M. Pollefeys, and R. Siegwart. Get out of my lab: Large-scale, real-time visual-inertial localization. In *Robotics: Science and Systems*, 2015. 2
- [39] W. Maddern, G. Pascoe, C. Linegar, and P. Newman. 1 year, 1000 km: The oxford robotcar dataset. *I. J. Robotics Res.*, 36:3–15, 2017. 2, 4
- [40] C. McManus, W. Churchill, W. P. Maddern, A. D. Stewart, and P. Newman. Shady dealings: Robust, long-term visual localisation using illumination invariance. *2014 IEEE International Conference on Robotics and Automation (ICRA)*, pages 901–906, 2014. 1, 3
- [41] S. Middelberg, T. Sattler, O. Untzelmann, and L. Kobbelt. Scalable 6-dof localization on mobile devices. In *ECCV*, 2014. 1
- [42] F. Radenovic, A. Iscen, G. Tolias, Y. S. Avrithis, and O. Chum. Revisiting oxford and paris: Large-scale image retrieval benchmarking. *CoRR*, abs/1803.11285, 2018. 3, 4
- [43] F. Radenovic, G. Tolias, and O. Chum. Fine-tuning cnn image retrieval with no human annotation. *IEEE transactions on pattern analysis and machine intelligence*, 2018. 2, 3, 4, 5, 6, 8
- [44] A. S. Razavian, J. Sullivan, A. Maki, and S. Carlsson. Visual instance retrieval with deep convolutional networks. *CoRR*, abs/1412.6574, 2014. 2, 3, 4
- [45] T. Sattler, M. Havlena, F. Radenovic, K. Schindler, and M. Pollefeys. Hyperpoints and fine vocabularies for large-scale location recognition. *2015 IEEE International Conference on Computer Vision (ICCV)*, pages 2102–2110, 2015. 2
- [46] T. Sattler, M. Havlena, K. Schindler, and M. Pollefeys. Large-scale location recognition and the geometric burstiness problem. *2016 IEEE Conference on Computer Vision and Pattern Recognition (CVPR)*, pages 1582–1590, 2016. 2
- [47] T. Sattler, B. Leibe, and L. Kobbelt. Efficient & effective prioritized matching for large-scale image-based localization. *IEEE Transactions on Pattern Analysis and Machine Intelligence*, 39:1744–1756, 2017. 2, 3, 6, 7, 8
- [48] T. Sattler, W. Maddern, C. Toft, A. Torii, L. Hammarstrand, E. Stenborg, D. Safari, M. Okutomi, M. Pollefeys, J. Sivic, F. Kahl, and T. Pajdla. Benchmarking 6DOF Outdoor Visual Localization in Changing Conditions. In *IEEE Conference on Computer Vision and Pattern Recognition (CVPR 2018)*, Salt Lake City, UT, United States, June 2018. 1, 2, 3, 4, 5, 6, 7, 8, 9
- [49] T. Sattler, C. Sweeney, and M. Pollefeys. On sampling focal length values to solve the absolute pose problem. In *ECCV*, 2014. 2
- [50] T. Sattler, A. Torii, J. Sivic, M. Pollefeys, H. Taira, M. Okutomi, and T. Pajdla. Are Large-Scale 3D Models Really Necessary for Accurate Visual Localization? In *CVPR 2017 - IEEE Conference on Computer Vision and Pattern Recognition*, page 10, Honolulu, United States, July 2017. 2, 3
- [51] J. L. Schönberger, M. Pollefeys, A. Geiger, and T. Sattler. Semantic visual localization. *CoRR*, abs/1712.05773, 2017. 2
- [52] G. Singh and J. Košecká. *Semantically Guided Geo-location and Modeling in Urban Environments*, pages 101–120. 2016. Exported from <https://app.dimensions.ai> on 2018/10/15. 2
- [53] L. Svärm, O. Enqvist, F. Kahl, and M. Oskarsson. City-Scale Localization for Cameras with Known Vertical Direction. *IEEE Transactions on Pattern Analysis and Machine Intelligence*, 39(7):1455–1461, 7 2017. 2, 6, 7, 8
- [54] L. Svärm, O. Enqvist, M. Oskarsson, and F. Kahl. Accurate localization and pose estimation for large 3d models. *2014 IEEE Conference on Computer Vision and Pattern Recognition*, pages 532–539, 2014. 2
- [55] H. Taira, M. Okutomi, T. Sattler, M. Cimpoi, M. Pollefeys, J. Sivic, T. Pajdla, and A. Torii. Inloc: Indoor visual localization with dense matching and view synthesis. *CoRR*, abs/1803.10368, 2018. 3
- [56] C. Toft, E. Stenborg, L. Hammarstrand, L. Brynte, M. Pollefeys, T. Sattler, and F. Kahl. Semantic match consistency for long-term visual localization. In *The European Conference on Computer Vision (ECCV)*, 09 2018. 2, 3, 6, 7, 8
- [57] G. Tolias, R. Sivic, and H. Jégou. Particular object retrieval with integral max-pooling of cnn activations. *CoRR*, abs/1511.05879, 2015. 2, 3, 4
- [58] A. Torii, R. Arandjelovic, J. Sivic, M. Okutomi, and T. Pajdla. 24/7 place recognition by view synthesis. *IEEE Transactions on Pattern Analysis and Machine Intelligence*, 40:257–271, 2015. 1, 2, 3, 4, 6, 7, 8

- [59] F. Walch, C. Hazirbas, L. Leal-Taixé, T. Sattler, S. Hilsenbeck, and D. Cremers. Image-based localization using lstms for structured feature correlation. *2017 IEEE International Conference on Computer Vision (ICCV)*, pages 627–637, 2017. [2](#)
- [60] K. M. Yi, E. Trulls, V. Lepetit, and P. Fua. Lift: Learned invariant feature transform. In *ECCV*, 2016. [2](#)
- [61] A. R. Zamir and M. Shah. Accurate image localization based on google maps street view. In *ECCV*, 2010. [2](#), [3](#)
- [62] B. Zeisl, T. Sattler, and M. Pollefeys. Camera pose voting for large-scale image-based localization. *2015 IEEE International Conference on Computer Vision (ICCV)*, pages 2704–2712, 2015. [2](#)
- [63] W. Zhang and J. Kosecka. Image based localization in urban environments. *Third International Symposium on 3D Data Processing, Visualization, and Transmission (3DPVT'06)*, pages 33–40, 2006. [2](#), [3](#)